Electronic Supplementary Material (ESI) for Journal of Materials Chemistry A.

Supplementary information

Zeolite-driven Ag species during redox treatments and catalytic implications for SCO of NH_3

Christian W. Lopes,[a]† Joaquín Martínez-Ortigosa,[a] Kinga Góra-Marek,[b] Karolina Tarach,[b] José A. Vidal-Moya,[a] Antonio E. Palomares,[a] Giovanni Agostini,[c] Teresa Blasco[a,*] and Fernando Rey[a]

[a]Instituto de Tecnología Química (Universitat Politècnica de València – Consejo Superior de Investigaciones Científicas), Avda. de Los Naranjos s/n, Valencia 46022, Spain.

[b]Faculty of Chemistry, Jagiellonian University in Kraków, 2 Gronostajowa St., Kraków 30-387, Poland.

[c]ALBA Synchrotron Light Source, Crta. BP 1413, Km. 3.3, Cerdanyola del Vallès 08290, Spain.

[*]Corresponding author. Email: tblasco@itq.upv.es

†Universidade Federal do Rio Grande do Sul, Instituto de Química, Laboratório de Reatividade e Catálise, Porto Alegre 91501-970, Brazil.

Table of contents

I. Experimental

Zeolites synthesis

Zeolite NaCsRHO (4) (Si/Al_{EDX} = 4.4, Si/Al_{ICP} = 4.3, Cs/Al_{ICP} = 0.21, Na/Al_{ICP} = 0.56) was synthesized following the procedure reported by Chatelain[1]. In this way, 0.94 g of crown ether 18-C-6, 0.705 g of CsOH and 0.34 g of NaOH were dissolved in 6.04 g of distilled water. Then, 1.32 g of sodium aluminate (54 wt. % Al_2O_3, 39 wt. % Na_2O) were added and the resulting mixture was stirred until a clear solution was formed. Subsequently, 10.5 g of colloidal silica (Ludox AS-40) were added and the resulting reaction mixture was stirred at room temperature for 24 h. The final gel composition was: 1.8 Na_2O: 0.3 Cs_2O: Al_2O_3: 10 SiO_2: 0.5 R: 100 H_2O where R is the crown ether 18-C-6 acting as organic structure-directing agent (OSDA). All chemicals were purchased from Sigma-Aldrich except sodium aluminate that was supplied by Carlo Erba. Zeolite crystallization was carried out in Teflon-lined stainless-steel autoclaves at 125 °C under rotation for 3 days. The solid recovered after filtration was washed with distilled water, dried at 100 °C and calcined at 500 °C for 3 h in order to remove the occluded organic material. For the preparation of AgNaRHO, the Cs^+ cations were fully exchanged by Na^+ cations using a solution of $NaNO_3$ (1 mol/L) with a solid/liquid ratio of 1/100 at room temperature for 16 h under mechanical stirring. The procedure was repeated until no Cs was detected. Then, silver was incorporated by ion exchange using the methodology described in the main text.

Zeolite KCHA(2) (Si/Al_{EDX} = 2.2, Si/Al_{ICP} = 2.2, K/Al_{ICP} = 0.99) was synthesized according to a published procedure,[2] in which Y zeolite (CBV500) was suspended in distilled water (64 mL) and an aqueous solution of potassium hydroxide (KOH; 9g; 98.5%; Fisher Chemicals) was added, resulting in a gel of chemical composition: 2.65 K_2O: 1.0 Al_2O_3: 4.8 SiO_2: 183 H_2O. The mixture was stirred for 1 h, then transferred into a polypropylene bottle and heated in the oven at 95 °C for 4 days. The solid product was recovered by filtration, washed with distilled water, and dried at 100 °C. The synthesis of KCHA(4) (Si/Al_{EDX} = 4.5, Si/Al_{ICP} = 3.8, K/Al_{ICP} = 0.78) was carried out by interzeolite conversion using FAU zeolite as Si and Al source and N,N,N-trimethyl-1-adamantammonium cation as OSDA, according to Zones.[3]

II. Figures

FIGURE S1

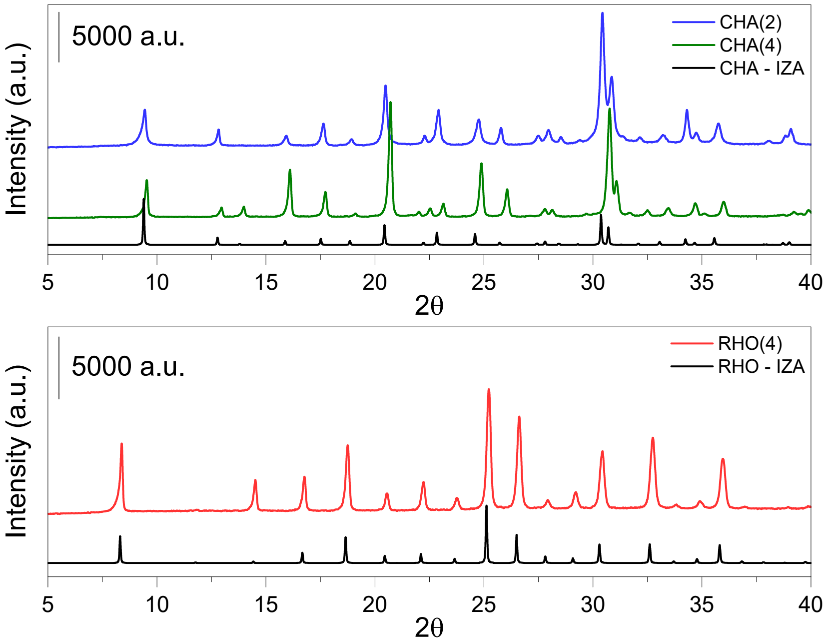

Figure S1. X-ray diffraction patterns of as-synthesized KCHA(2), KCHA(4) and NaCsRHO(4) zeolites compared with the CHA and RHO profiles obtained from IZA.[4]

The XRD patterns of as-synthesized KCHA(2), KCHA(4) and NaCsRHO(4) zeolites are similar to the simulated pattern obtained from the IZA database, without the presence of concurring or dense phases (e.g. quartz or cristobalite).

FIGURE S2

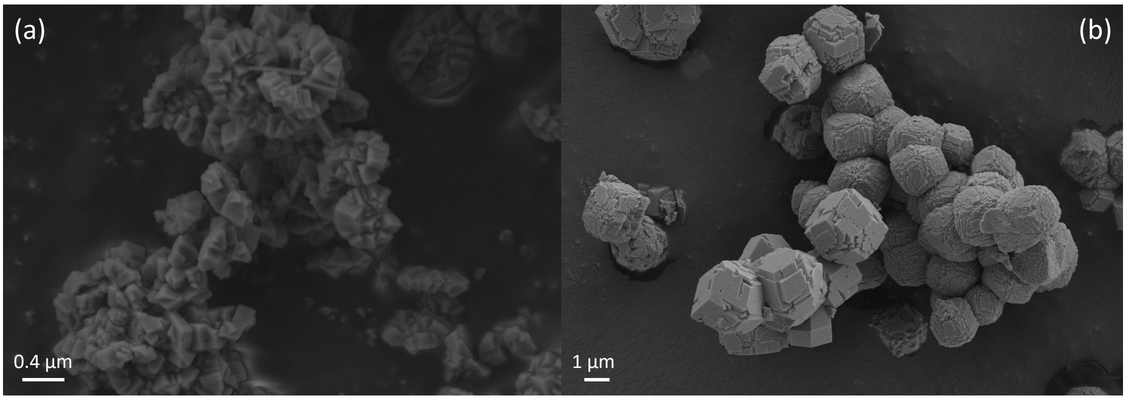

Figure S2. FESEM images of CHA(2) (a) and RHO(4) (b) zeolites.

The morphology of the NaCsRHO(4) and KCHA(2) samples shown in the FESSEM images of **Figure S2** are typical of the RHO and CHA type structures, respectively. The NaCsRHO sample presents cubic crystals with homogeneous size of ca. 2-4 µm, while the KCHA zeolite crystals consist of an intergrowth of spiral-shaped crystals smaller than 1 µm. The EDX analysis taken during FESEM measurements confirm the Si/Al ratios determined by chemical analysis (**Table 1**).

FIGURE S3

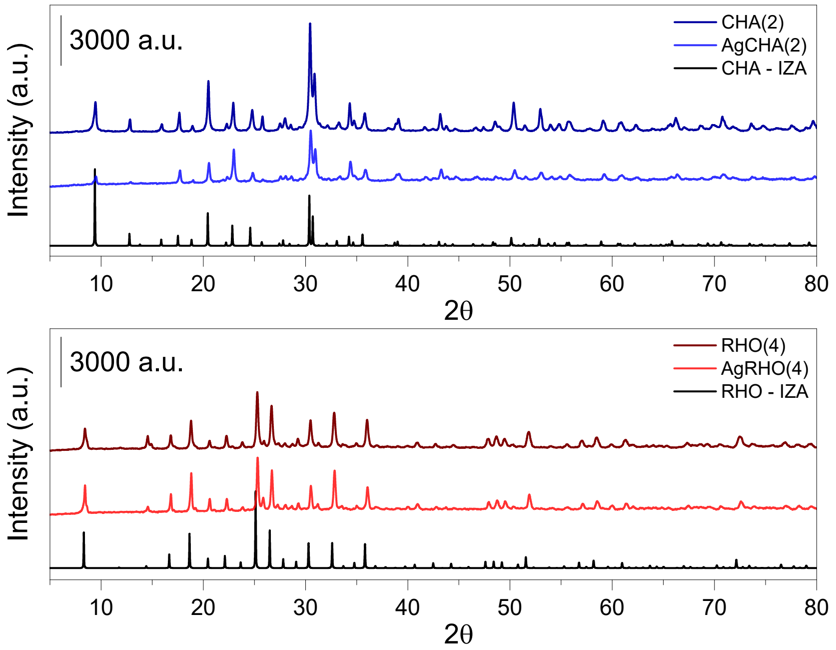

Figure S3. X-ray diffractograms of (a) CHA(2), AgCHA(2) and (b) RHO(4) and AgRHO(4) compared with the CHA and RHO profiles obtained from IZA.[4]

The X-ray diffractograms of the Ag exchanged zeolites are similar to those of the as-synthesized zeolites indicating that the structures have not been modified.

FIGURE S4

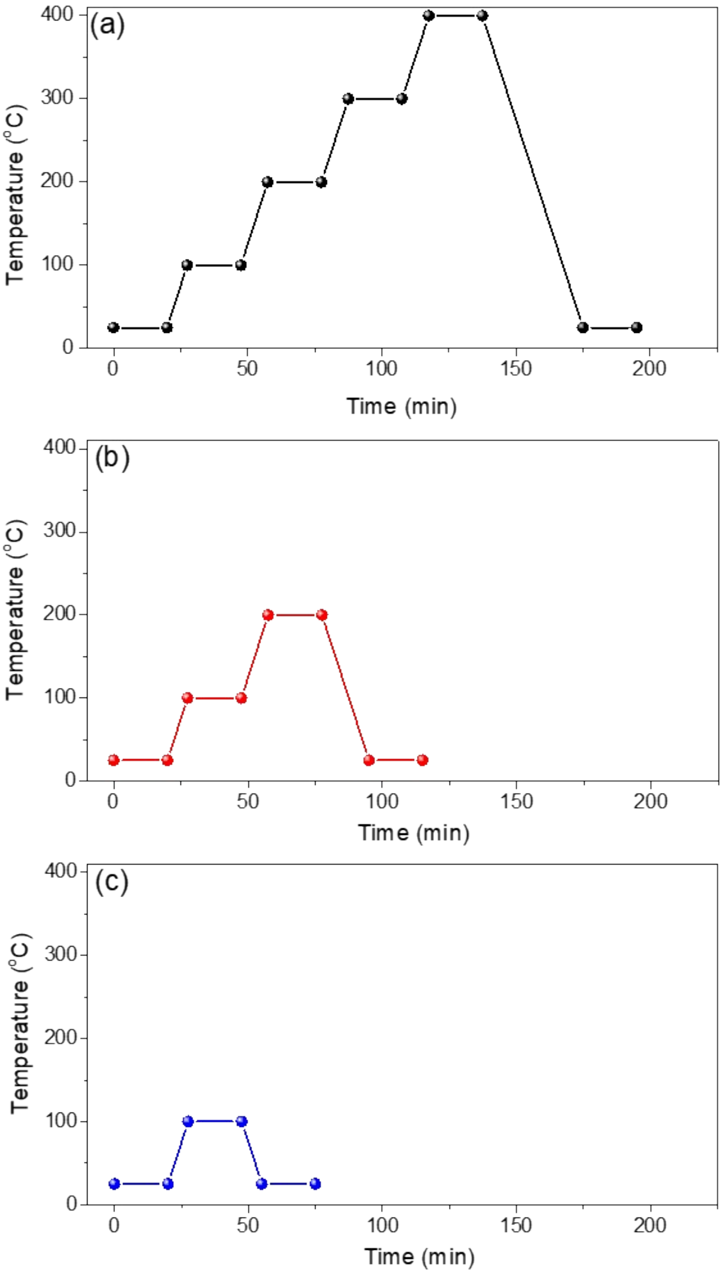

Figure S4. Experimental steps used in the XAS study of Ag-containing zeolites: treatment at 400 ºC (a), 200 ºC (b) and 100 ºC (c).

FIGURE S5

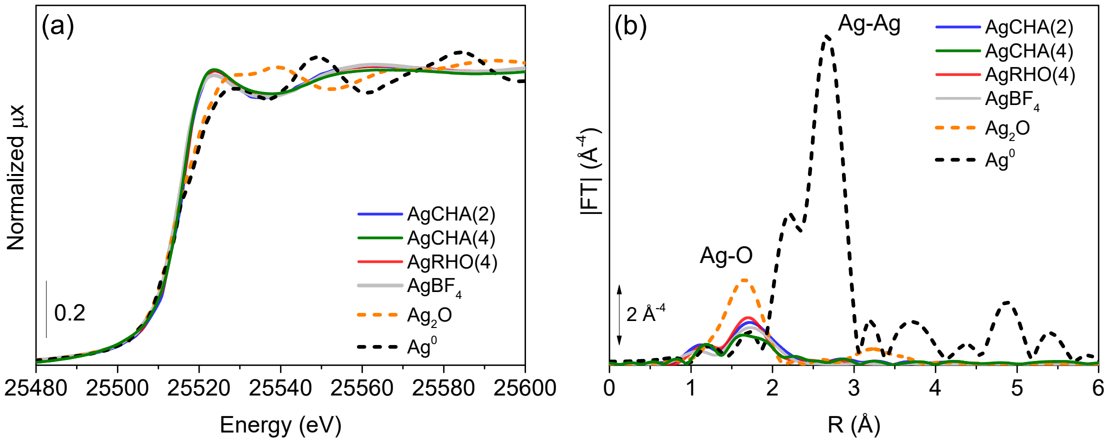

Figure S5. Normalized XANES (a) |FT| of the k^3-weighted EXAFS spectra (b) of as-prepared AgCHA(2), AgCHA(4) and AgRHO(4) zeolites and the the Ag foil, $AgBF_4$, and bulk Ag_2O standards.

Figure S5a and 5b shows the XANES spectra and the |FT| of k^3-weighted $\chi(k)$ signals at the Ag K-edge, of the AgCHA(2), AgCHA(4) and AgRHO(4) zeolites, as well as those of the Ag foil, $AgBF_4$, and bulk Ag_2O standards. The XANES and the |FT| spectra of the Ag-zeolites are similar to that of $AgBF_4$, indicating that silver is as Ag^+ ion. The |FT| spectra of **Figure S5b** show a prominent peak centered at 1.7 Å (not corrected in phase) attributed to Ag–O. The peak of Ag–O of Ag_2O, is less intense and slightly shifted to a shorter distance, confirming that in Ag-zeolites silver is as highly dispersed Ag^+ and not in the form of oxide.

FIGURE S6

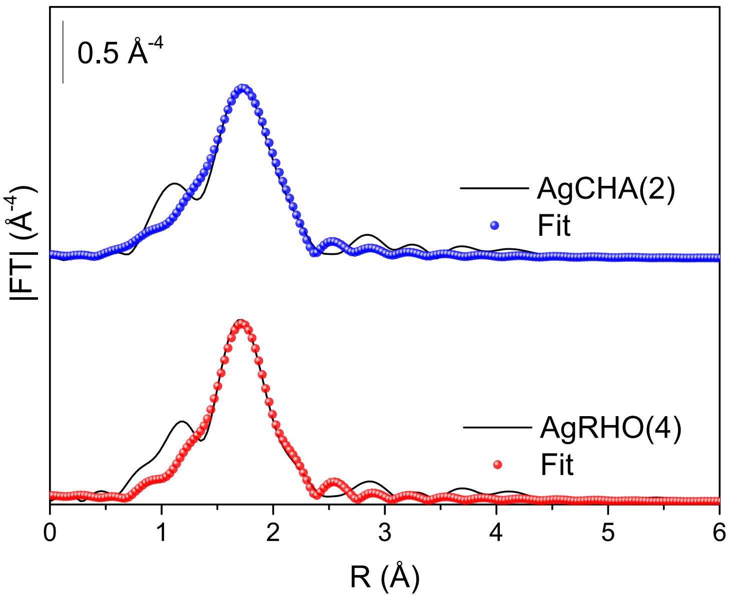

Figure S6. Curve-fittings and |FT| of the k^3-weighted $\chi(k)$ functions of as-prepared AgCHA(2) and AgRHO(4) zeolites. Solid lines refer to experimental data and colored circles represents the fit.

The first shell of the |FT| data for the AgCHA(2) and AgRHO(4) samples was simulated by the convolution of two Ag–O distances at 2.26 Å and 2.43 Å with an average coordination number close to 3 (see **Table S1**).

FIGURE S7

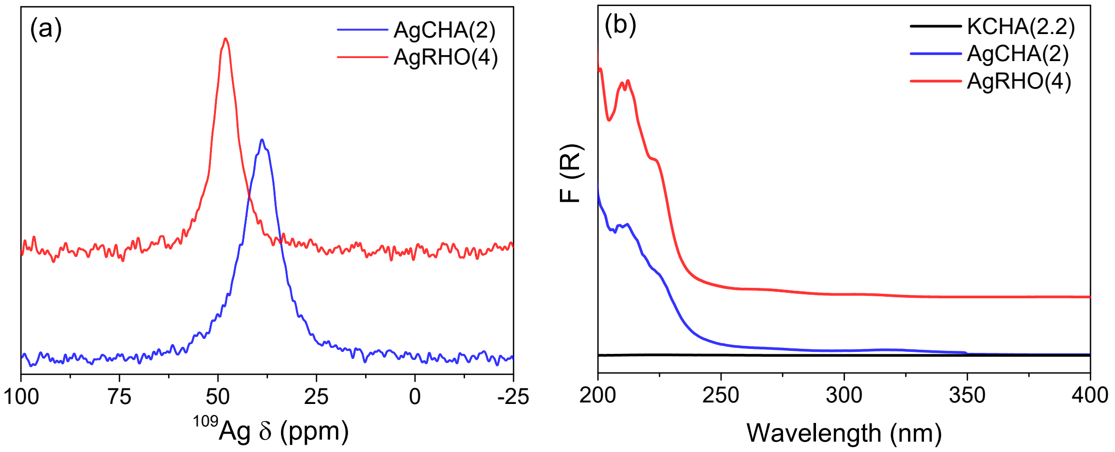

Figure S7. ^{109}Ag MAS NMR (a) and UV-Vis spectra (b) of as-made KCHA(2.2), AgCHA(2) and AgRHO(4) zeolites.

Figure S7a shows the ^{109}Ag MAS NMR spectra of the AgCHA(2) and AgRHO(4) zeolites which consist of a signal at δ^{109}Ag ≈ 25-50 ppm of Ag^+ in zeolites. **Figure S7b** shows the corresponding UV-vis spectra which exhibit a band at 210 nm attributed to the charge transfer transition between $4d^{10}$ and $4d^{9}5s^{1}$ levels of highly dispersed Ag^+ cations.[5] The spectra indicate that the contribution of the KCHA(2.2) (Ag-free zeolite) in the UV-Vis spectrum is negligible.

FIGURE S8

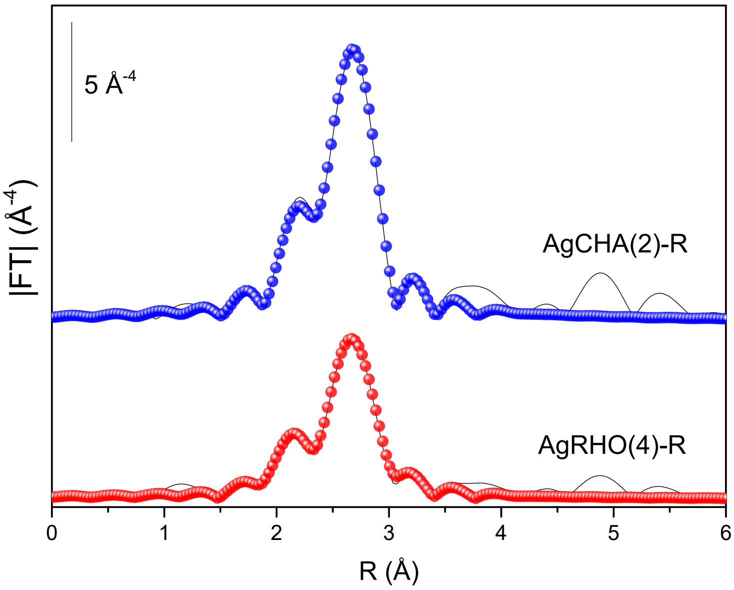

Figure S8. Curve-fittings and |FT| of the k^3-weighted χ(k) functions of AgCHA(2)-R (top) and AgRHO(4)-R (bottom) zeolites. Solid lines refer to experimental data while colored circles represent the fits.

The results corresponding to the curve-fittings shown of **Figure S8** are collected in **Table S2**. The coordination numbers of the zeolites reduced at 400 ºC are close to that of metal foil ($N_{Ag\text{-}Ag}$ = 12) for the AgCHA(2) and significantly smaller (about 8.6) for the AgRHO(4).

FIGURE S9

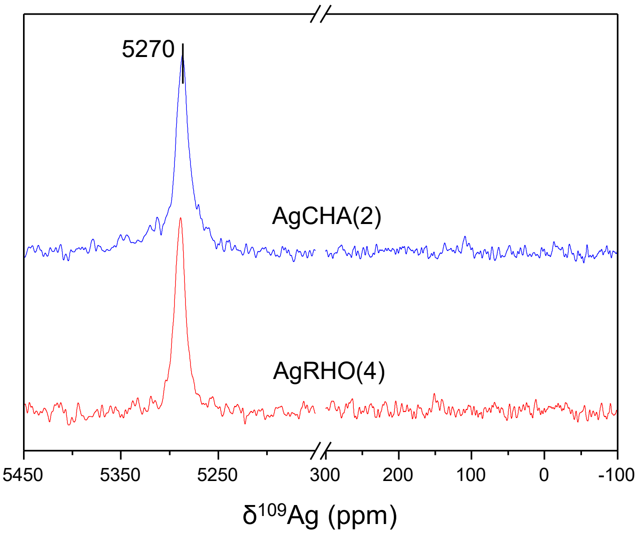

Figure S9. ^{109}Ag MAS NMR spectra of reduced AgCHA(2) and AgRHO(4) zeolites. Note the absence of any signal in the high field region corresponding to Ag^{+}.

FIGURE S10

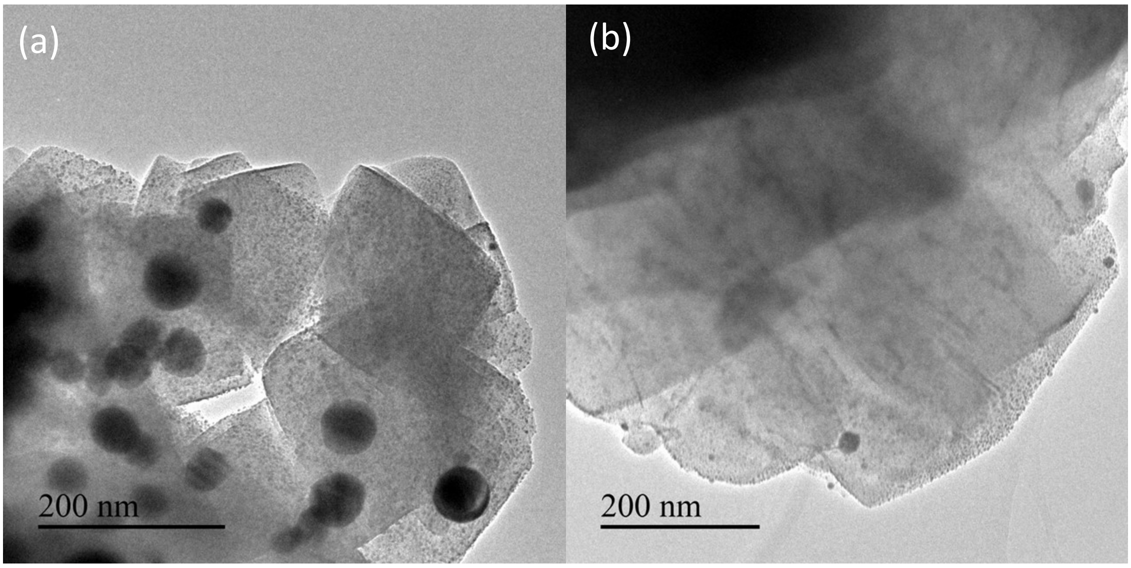

Figure S10. TEM images of AgCHA(2)-R (a) and AgRHO(4)-R (b).

FIGURE S11

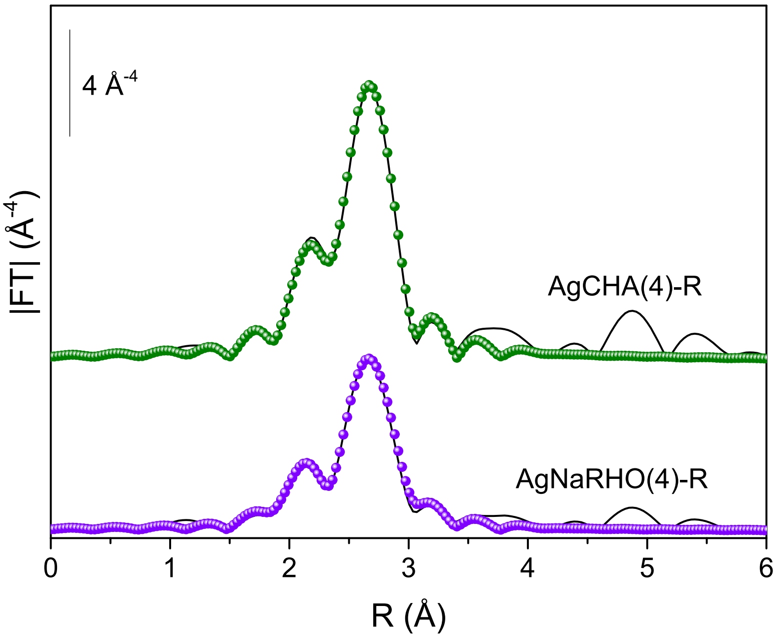

Figure S11. Curve-fittings and |FT| of the k^3-weighted $\chi(k)$ functions of AgCHA(4) and AgNaRHO(4) zeolites reduced at 400 ºC. Solid lines refer to experimental data while colored circles represent the fits.

FIGURE S12

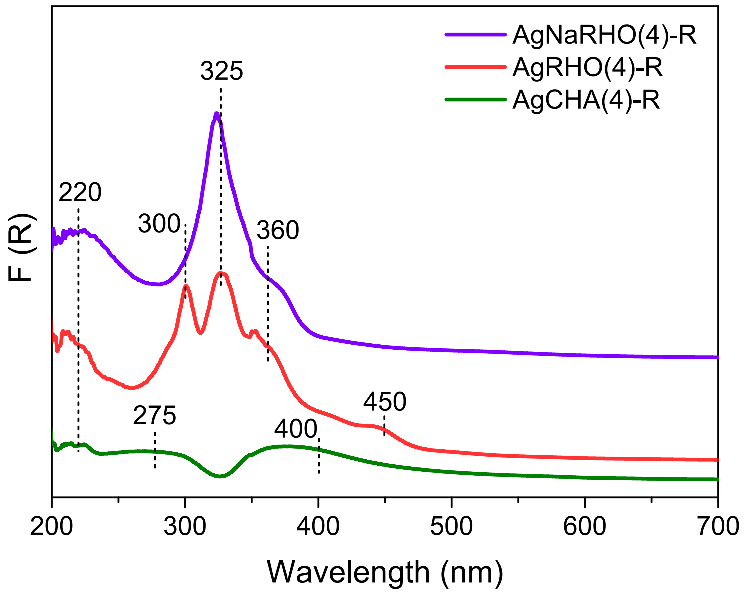

Figure S12. UV-Vis spectra of reduced AgCHA(4), AgRHO(4) and AgNaRHO(4) zeolites.

FIGURE S13

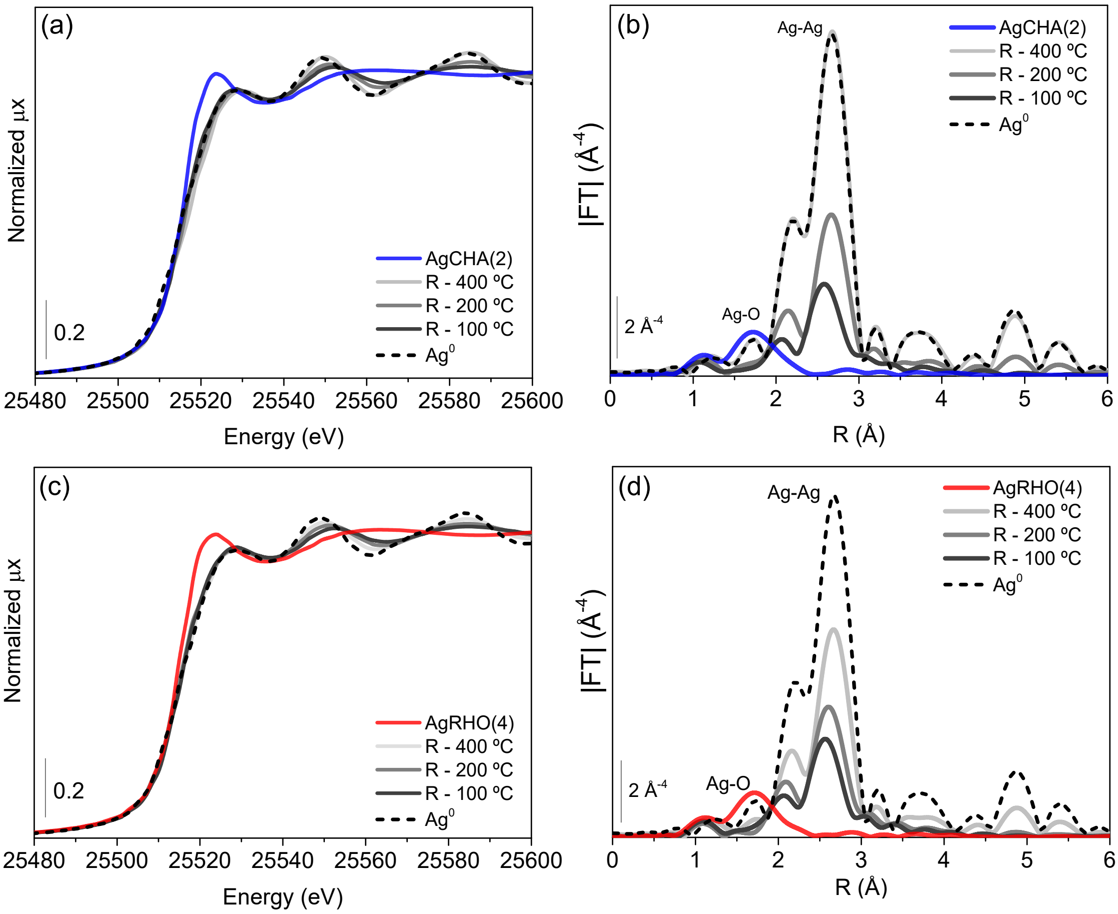

Figure S13. Normalized XANES spectra (left side) and |FT| of the k^3-weighted EXAFS spectra (right side) of AgCHA(2) (a-b) and AgRHO(4) (c-d) zeolites after reduction treatments. The reduced samples were cooled down to RT under H_2 atmosphere before data collection to minimize DWF and allow direct comparison.

Figure S13a and S13c show the normalized XANES spectra of the AgCHA(2) and AgRHO(4) zeolites, respectively, reduced at 100 ºC, 200 ºC and 400 ºC compared with the as-prepared samples and the Ag^0 foil. All absorption edges appear at the same position (E_0 at 25514 eV). Meanwhile, the white lines of the treated zeolites are less intense than for the as-prepared samples and shifted to the right resembling that of Ag^0, indicating the reduction of Ag^+ to Ag^0. For the samples reduced at 100 ºC and 200 ºC, the oscillations beyond the absorption edge are more flattened and shifted to around 25560 eV, indicating silver atoms in low coordination and thus the occurrence of small metal nanoparticles, and the same accounts for the AgRHO(4) zeolite reduced at 400 ºC (zeolite AgRHO(4)-

R). Meanwhile, the spectra of the AgCHA zeolites reduced at 400 ºC (AgCHA(2)-R and AgCHA(4)-R) fit that of Ag^0 metal, indicating large particle sizes. **Figure S13b** and **S13d** show the |FT| spectra of the AgCHA(2) and AgRHO(4) zeolites reduced at 100 ºC, 200 ºC and 400 ºC, respectively. The spectra show only a peak centered at about 2.6 Å due to Ag−Ag bond, whose intensity increases and shifts to longer distances (not phase corrected) as the reduction temperature increases. After reduction at 400 ºC, the spectra of the two AgCHA zeolites are similar to that of metal foil, whereas the intensity of the Ag−Ag peak of the spectrum of the AgRHO(4) zeolite is lower (see **Table S2**).

FIGURE S14

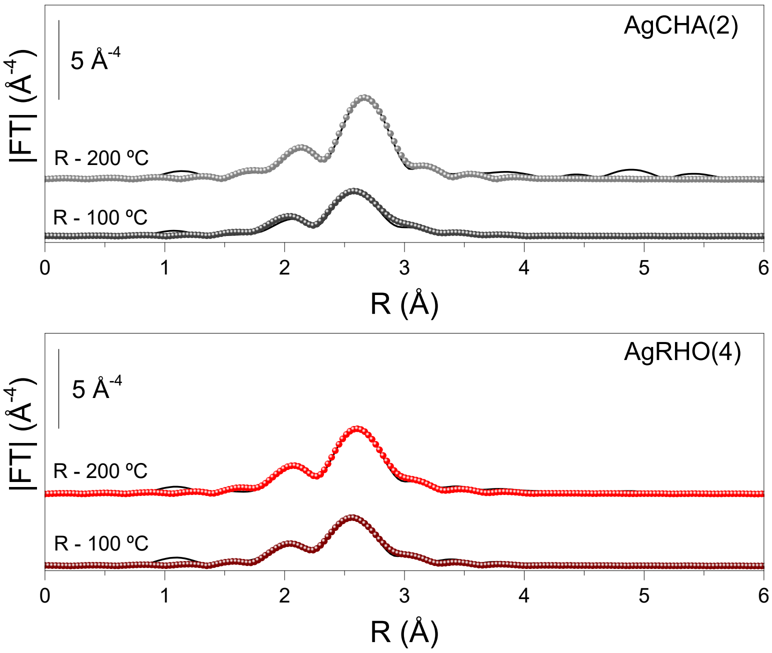

Figure S14. Curve-fittings and |FT| of the k^3-weighted $\chi(k)$ functions of AgCHA(2) (top) and AgRHO(4) (bottom) zeolites reduced at 100 ºC and 200 ºC. Solid lines refer to experimental data while colored circles represent the fits.

The results corresponding to the curve-fittings shown of **Figure S14** are collected in **Table S2**.

FIGURE S15

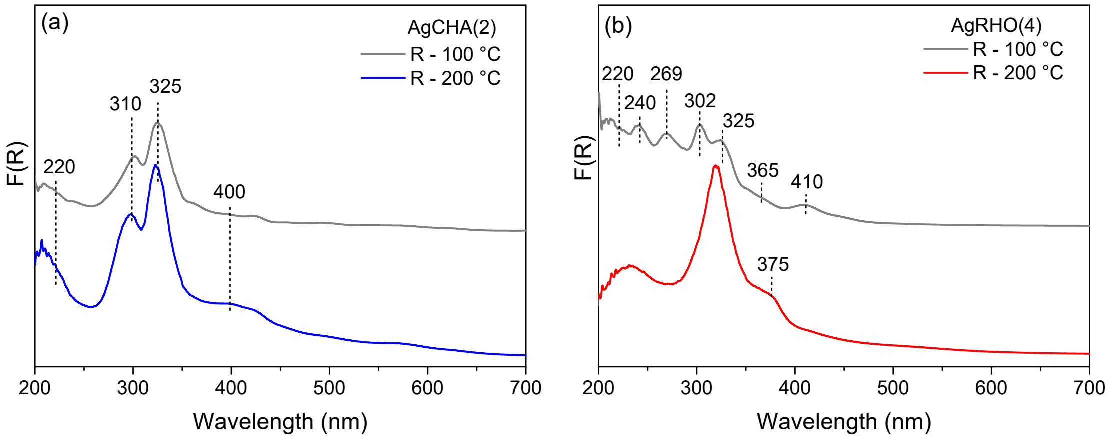

Figure S15. *Ex situ* UV-Vis spectra of AgCHA(2) (a) and AgRHO(4) (b) zeolites reduced at 100 °C and 200 °C.

The UV-Vis spectra of the AgCHA(2) reduced at 100 °C and 200 °C show bands at 310 nm and 325 nm previously ascribed to silver clusters of Ag_8-type and a broad and weak band at ≈ 400 nm assigned to metal particles, more intense at 200 °C.[6-7] The spectrum of the AgRHO(4) zeolite reduced at 100 °C displays the bands at $\lambda = 240$ nm and $\lambda = 269$ nm assigned to $Ag_m^{\delta+}$ and at 310 nm and 325 nm assigned to Ag_8 clusters. Meanwhile the spectrum of the AgRHO(4) reduced at 200 °C is dominated by the band at 325 nm assigned to Ag_8 clusters. [36]

FIGURE S16

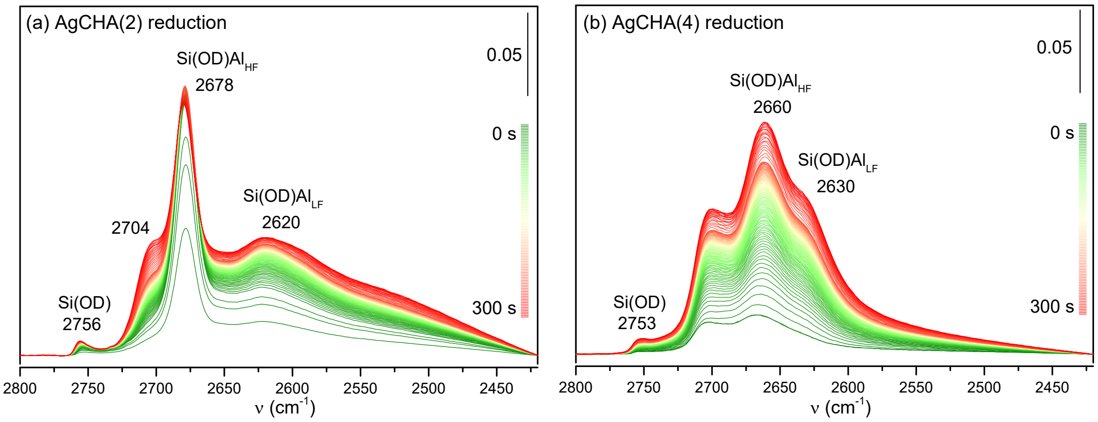

Figure S16. (a-b) Time-resolved rapid scan FT-IR spectra in the region of O-D stretching vibrations of the AgCHA zeolites contacted with D_2 at 200 ºC for 5 min.

Figure S16 shows the rapid scan FT-IR spectra recorded under *operando* conditions upon heating at 200 ºC with D_2 the AgCHA(2), AgCHA(4) zeolites, taking one spectrum every 0.6 seconds. The reduction of Ag^+ to Ag^0 is accompanied by the appearance of Si(OD)Al$_{HF}$ (HF) and Si(OD)Al$_{LF}$) (LF) bands in the 2800-2450 cm^{-1} region, which are associated to different oxygen sites in the zeolite framework and appear at a slightly different frequency for the AgCHA(2), AgCHA(4) and AgRHO(4) zeolites (see **Figure 5** in the main text). The amount of the Si(OD)Al groups was calculated by applying the respective absorption coefficient (3.35 cm·µmol^{-1}) to the spectra of the reduced samples recorded after deuterium evacuation. The FT-IR spectra also show a band at around 2704 cm^{-1} tentatively assigned to OD groups associated to pre-existent hydroxyl groups bonded to the zeolite.[8]

FIGURE S17

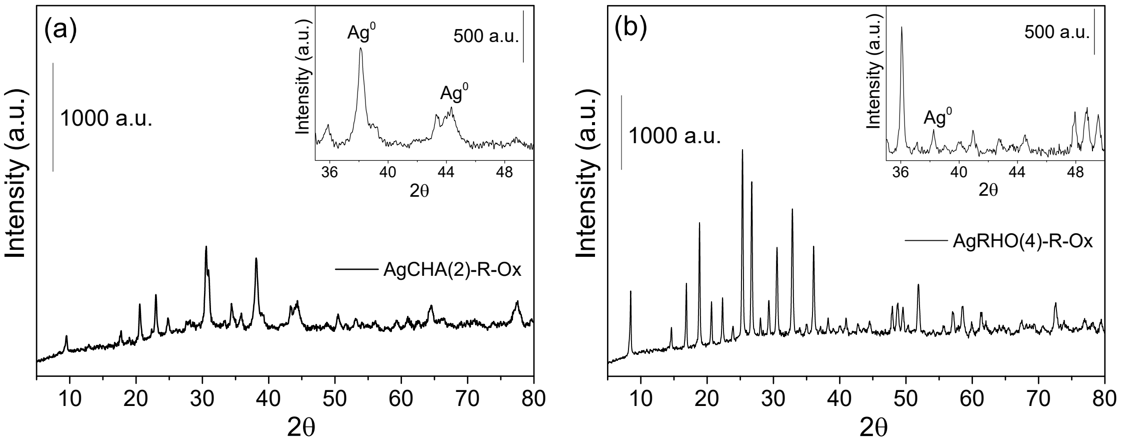

Figure S17. XRD patterns of an the AgRHO(4) (a) AgCH(2) (b) zeolites after reduction and subsequent reoxidation at 400 °C. Inset: selected 2θ range for better visualization of Ag^0 peaks.

FIGURE S18

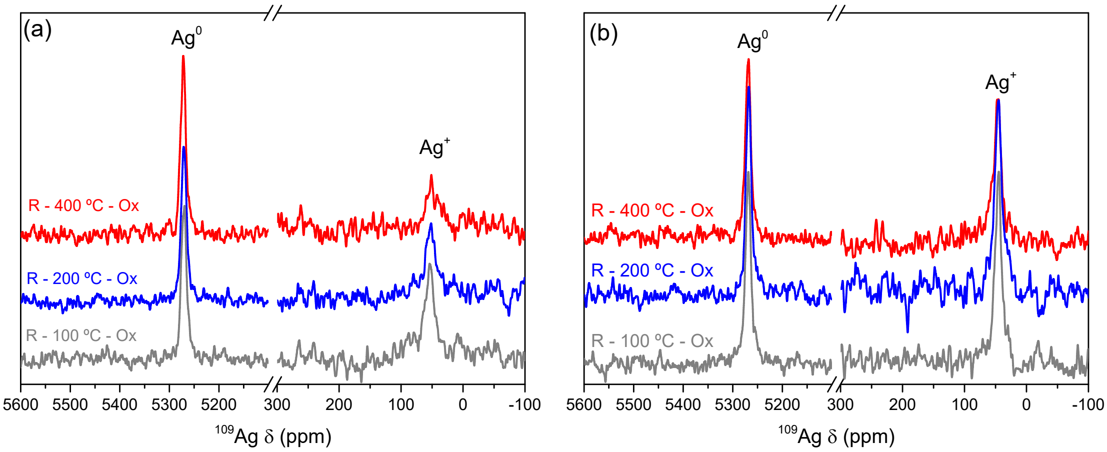

Figure S18. ^{109}Ag MAS NMR spectra of reduced and re-oxidized AgCHA(2) (a) and AgRHO(4) (b) zeolites.

Figure S18 displays the ^{109}Ag NMR spectra of the AgRHO(4) and AgCHA(2) zeolites reduced at 100 °C, 200 °C and 400 °C and then oxidized at 400 °C. The spectra show two peaks at δ ^{109}Ag ≈ 5270 ppm and δ ^{109}Ag ≈ 39 – 47 ppm assigned to Ag^0 and Ag$^+$, respectively. The relative intensity of the peak of Ag$^+$ is higher for the samples pre-reduced at a lower temperature and for the AgRHO(4) zeolite. The peak of Ag^0 in the spectrum of the AgCHA(2) zeolite pre-reduced at 400 °C and then oxidized is narrower than that of silver metal, suggesting smaller metal nanoparticles than in the reduced sample.

FIGURE S19

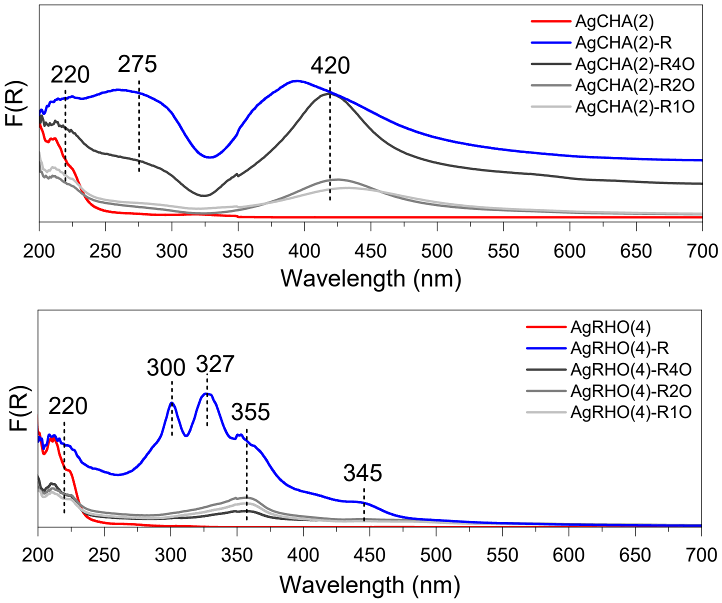

Figure S19. UV-Vis spectra of AgCHA(2) (top) and AgRHO(4) (bottom) zeolites reduced at 100 °C, 200 °C and 400 °C and then oxidized at 400 °C noted in the figure as -R1O, -R2O and -R4O, respectively. The spectra of the zeolites as-prepared and reduced at 400 °C (-R) are also included for comparison.

Figure 19a and **Figure 19b** show the UV-Vis spectra recorded after oxidizing at 400 °C the AgCHA(2) and AgRHO(4) zeolites, respectively, pre-reduced at 100 °C, 200 °C and 400 °C. The spectra of the AgCHA(2)-R1-Ox and - R2-Ox zeolites show the bands at 420 nm assigned to silver metal and at 220 nm due to highly dispersed Ag^+ cation.[5] Meanwhile, the spectra of the AgRHO(4)-R1-Ox and AgRHO(4)-R2-Ox zeolites display mainly the band of Ag^+ species and another very weak centered at 355 nm attributed to small Ag^0 nanoparticles.[9]

FIGURE S20

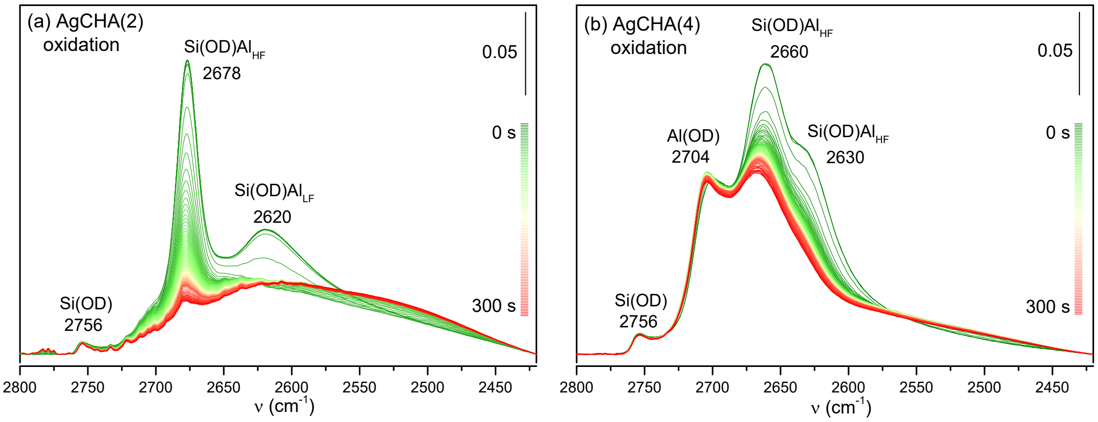

Figure S20. (a-b) Time-resolved rapid scan FT-IR spectra in the region of O-D stretching vibrations of the AgCHA zeolites studied contacted with O_2 at 200 °C for 5 min.

Figure S20 shows the FT-IR spectra under *operando* conditions during the treatment with O_2 at 200 °C of the AgCHA(2) and AgCHA(4) zeolites submitted to the experiment depicted in **Figure S16** (reduced with D_2 at 200 °C). The intensity of the Si(OD)Al groups monitored by FT-IR (2680-2620 cm^{-1}) decreases as Ag^0 is oxidized to Ag^+. The spectra of the AgCHA zeolites show a very broad band at about 2550 cm^{-1}, more intense for AgCHA(2), that increases with time indicating the formation of water during the oxidation process. According to the evolution of the Si(OD)Al bands, the oxidation of Ag^0 to Ag^+ occurs within 5 min for the two AgCHA zeolites. The Si(OD)Al$_{LF}$ band (2620 cm^{-1}) observed in the spectra of the AgCHA(2) disappears in the earlier oxidation period, suggesting that the bridging hydroxyls situated in the 6-ring prism (a member of two four-membered rings and one six-membered ring) are replaced by Ag^+ in the first stages.[10-11] It must be noted Al(OD) band present in the spectra of the AgCHA(4) zeolite do not completely disappear upon oxidation, probably because it can be due to Brønsted acid sites already present in the as-prepared sample.

FIGURE S21

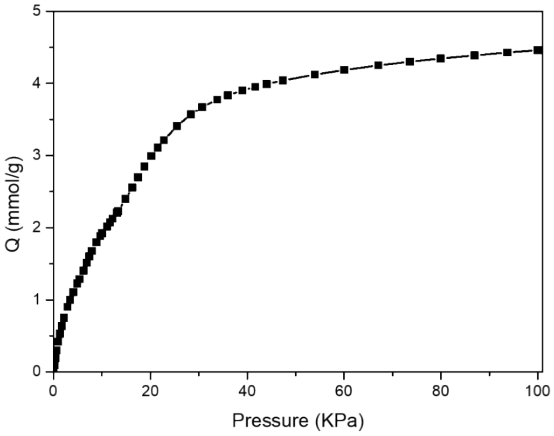

Figure S21: CO_2 adsorption isotherm at 0 °C on AgRHO(4)-R.

Prior to the adsorption experiment, the AgRHO(4)-R zeolite was outgassed at 400 °C overnight. The sample was mounted on an ASAP 2020 from Micromeritics and the isotherm was measured at 0 ± 0.01 °C by maintaining the temperature using a recirculating thermostatic bath (Julabo F25-HE).

FIGURE S22

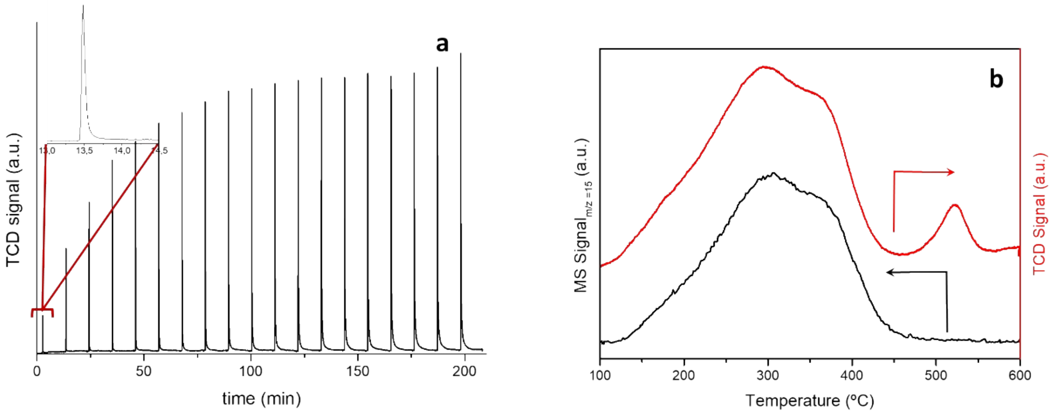

Figure S22: Ammonia adsorption-TPD-MS on sample AgRHO(4)-R. a) Pulsed ammonia adsorption experiment. b) TPD-MS profile (m/z = 15)

The AgRHO(4)-R zeolite adsorbs 23 STP cm^3/g, corresponding to a NH_3/Al molar ratio of 0.60, at 100 °C, which is similar to that obtained on a commercial Mordenite CBV-21 (Zeolyst Int) that gives a NH_3/Al molar ratio of 0.69. The experiment was achieved by pulse adsorption method (**Figure S22a**) so that the shape of each pulse gives an idea of the diffusional restrictions of NH_3 to enter the zeolite porosity. Adsorption on Ag-RHO(4)-R occurs in less than 45 second indicating that there is no significant diffusional limitations for NH_3 in the sample at 100 °C. The ammonia TPD profile (**Figure S22b**) gives information about the strength of the acid sites of the sample. The m/e = 15, which is characteristic of ammonia and does not fit with any water fragment, was followed while increasing the desorption temperature. There, two desorption features, one maximum circa 310 °C with a shoulder at 360 °C, prove the acid properties of the Ag-RHO(4)-R catalyst and the accessibility to ammonia molecules. The presence of the high temperature feature at 525 °C in the TCD signal is assigned to the evolution of water, since there is no signal al the m/z=15 plot. These results agree with prior publications describing the adsorption of ammonia on Ag species in zeolite RHO.[12]

FIGURE S23

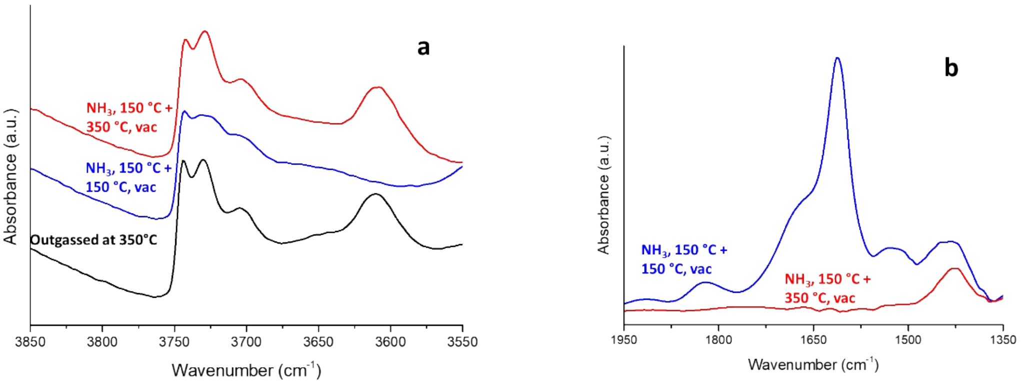

Figure S23: Ammonia adsorption-stepwise desorption on zeolite AgRHO(4)-R studied by IR spectroscopy. a) O–H stretching vibration region of the sample outgassed at 350 °C under vacuum (black), and subsequently saturated at 150 °C with ammonia and then, outgassed at 150 °C (blue) and 350 °C (red). b) Difference IR spectra in the N–H bending vibration region after ammonia saturation at 150 °C and desorption at 150 °C (blue) and 350 °C (red) under high vacuum (better than 10^{-4} mbar).

Ammonia adsorption and stepwise temperature desorption experiment supports the full access of ammonia to the acid sites located inside of the AgRHO(4)-R catalyst. The IR spectrum of the dehydrated AgRHO(4)-R sample (**Figure S23a**) shows three bands at 3741, 3728 and 3708 cm^{-1} assigned to weakly acidic silanol groups. More relevant is the presence of one IR band at 3610 cm^{-1} characteristic of Brønsted acid Si–OH–Al groups.[13] The band assigned to Brønsted acid sites disappears upon adsorption of ammonia at 150 °C followed by high vacuum pumping at this temperature (to remove physisorbed ammonia), which is accompanied by the appearance of two bands in the bending N–H region (**Figure S23b**). One appears at 1621 cm^{-1}, which is assigned to ammonia linked to Lewis acid sites, and a second one at 1430 cm^{-1} that is assigned to ammonium cations formed by reaction with Brønsted acid centres.[13] Thus, the IR results show that the Ag-RHO(4)-R zeolite possesses Brønsted acid sites (bridging hydroxyl groups) and Lewis acid sites that can be tentatively assigned to the of cationic species. These cationic species are unable to retain ammonia at 350 °C and only a small fraction of Brønsted acid sites retains ammonia at this temperature (**Figure S23b**), while most of the intensity of the band assigned to Si−OH−Al is recovered (**Figure S23a**).

FIGURE S24

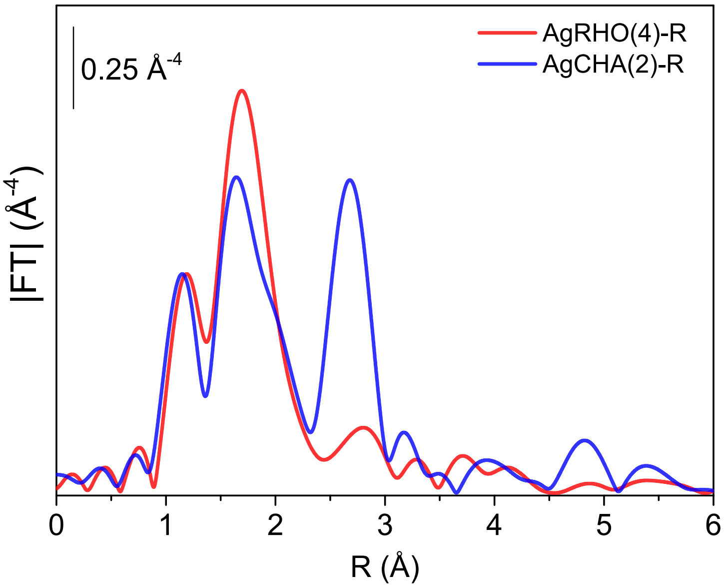

Figure S24. |FT| of the k^3-weighted χ(k) functions of AgCHA(2)-R and AgRHO(4)-R after catalysis.

FIGURE S25

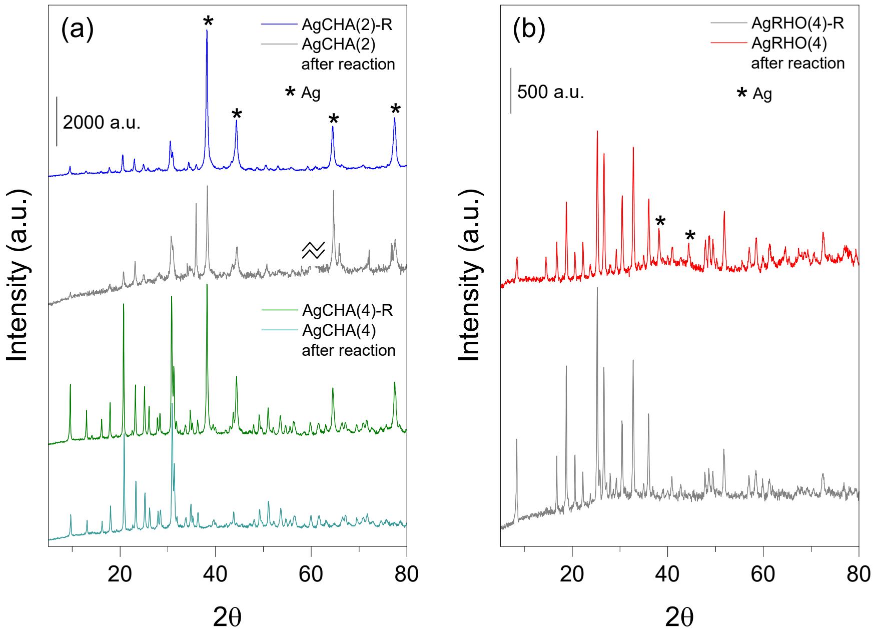

Figure S25. X-ray diffractograms of AgCHA (a) and AgRHO (b) zeolites in their reduced state and after catalysis. The diffractograms of the AgCHA(4) zeolite after reaction is interrupted in the 59–61° region to avoid the very intense peak corresponding to the SiC used as reaction diluent that makes difficult the observation of the diffraction peak of the zeolite and silver.

III. Tables

Table S1. Summary of EXAFS fit of the as-prepared Ag-loaded zeolites.[a]

Sample	CN	Path	R (Å)	σ^2 (Å^2)	ΔE_0 (eV)	r-factor
AgRHO(4)	1.6(4)	Ag-O	2.265(26)	0.0060(35)	2.5(2.2)	0.0455
	1.2(2)		2.432(36)			
AgCHA(2)	1.7(2)	Ag-O	2.269(40)	0.0082(52)	1.6(2.6)	0.0567
	1.7(2)		2.427(43)			

[a]Fits were performed on the first coordination shell (ΔR = 1.1-3.0 Å) over FT of the k^3-weighted $\chi(k)$ functions performed in the Δk = 2.3-11.8 Å^{-1} interval, resulting in a number of independent parameters of $2\Delta R\Delta k/\pi = 11.2$. Non-optimized parameters are recognizable by the absence of the corresponding error bar. $S_0^2 = 0.80$.

Table S1 summarizes the results obtained from the simulation of the first shell of the |FT| data for the AgCHA(2) and AgRHO(4) samples (see **Figure S6**) by the convolution of two Ag–O distances at 2.26 Å and 2.43 Å with an average coordination number close to 3. The introduction of an Ag–T (T = Si or Al) path in the fit provides results with no physical meaning and no Ag–Ag or Ag–K(Cs) contributions are observed. Similar results with Ag–O distances in the 2.29 Å – 2.32 Å range and comparable $N_{Ag\text{-}O}$ have been reported by our group for AgLTA zeolites.[14] The contribution of oxygen atoms from water molecules cannot be ruled out since the measurements were performed on the hydrated samples.

Table S2. Summary of EXAFS fit of the reduced Ag-loaded zeolites.[a]

Sample	**CN**	**R (Å)**	**σ^2 (Å^2)**	**ΔE_0 (eV)**	**C_3 (Å^3)**	**r-factor**
AgCHA(2)$_{RED400}^{b}$	11.1(8)	2.852(12)	0.0093(6)	2.0(5)	-	0.0045
AgCHA(2)$_{RED200}^{b}$	7.6(8)	2.837(16)	0.0127(11)		-	0.0148
AgCHA(2)$_{RED100}$	5.1(5)	2.828(17)	0.0144(14)		0.0007(3)	0.0577
AgRHO(4)$_{RED400}^{b}$	8.6(7)	2.850(14)	0.0114(9)		-	0.0085
AgRHO(4)$_{RED200}$	6.6(6)	2.835(15)	0.0134(11)		0.0006(3)	0.0221
AgRHO(4)$_{RED100}$	4.5(5)	2.817(18)	0.0126(15)		0.0007(3)	0.0550
AgCHA(4)$_{RED400}^{c}$	11.3(6)	2.857(2)	0.0102(5)	1.5(2)	-	0.0029

[a] The fits were performed on the first coordination shell (ΔR = 2.0-3.0 Å) over FT of the $k^1k^2k^3$-weighted $\chi(k)$ functions performed in the Δk = 2.3-11.8 Å^{-1} interval, resulting in a number of independent parameters of $2\Delta R\Delta k/\pi$ = 34.3 without C_3. S_0^2 = 0.80 [b] Values obtained without C_3 fitting Ag metal reference. [c] Fit separately.

Table S2 collects the results obtained from the simulation of the Ag–Ag shell of the |FT| data of the AgCHA(2) and AgRHO(4) samples reduced at 100 °C, 200 °C (see **Figure S14**) and 400 °C (see **Figure S6**). The Ag–Ag coordination increases and the Debye-Waller factor decrease as the reduction temperature rises for the two samples. The coordination numbers of the AgCHA zeolites reduced at 400 °C are close to that of metal foil ($N_{Ag\text{-}Ag}$ = 12), while it is significantly smaller (about 8.6) for the AgRHO(4). Thus, the silver clusters/NPs sinter upon heating under H_2 flow at increasing temperatures in the 100 °C – 400 °C range.

IV. References

1. Chatelain, T.; Patarin, J.; Fousson, E.; Soulard, M.; Guth, J. L.; Schulz, P., Synthesis and characterization of high-silica zeolite RHO prepared in the presence of 18-crown-6 ether as organic template. *Microporous Mater.* **1995,** *4* (2-3), 231-238.
2. Ridha, F. N.; Yang, Y.; Webley, P. A., Adsorption characteristics of a fully exchanged potassium chabazite zeolite prepared from decomposition of zeolite Y. *Microporous Mesoporous Mater.* **2009,** *117* (1-2), 497-507.
3. Zones, S. I., Conversion of faujasites to high-silica chabazite SSZ-13 in the presence of N,N,N-trimethyl-1-adamantammonium iodide. *J. Chem. Soc., Faraday Trans.* **1991,** *87* (22), 3709-3716.
4. International Zeolite Association (IZA) webpage. http://www.iza-structure.org/databases/ (accessed 18/02/2021).
5. Yumura, T.; Oda, A.; Torigoe, H.; Itadani, A.; Kuroda, Y.; Wakasugi, T.; Kobayashi, H., Combined Experimental and Computational Approaches To Elucidate the Structures of Silver Clusters inside the ZSM-5 Cavity. *J. Phys. Chem. C* **2014,** *118* (41), 23874-23887.
6. Gurin, V. S.; Bogdanchikova, N. E.; Petranovskii, V. P., Few-Atomic Silver Clusters in Zeolites: Ab Initio MO LCAO Calculation and Optical Spectroscopy. *J. Phys. Chem. B* **2000,** *104* (51), 12105-12110.
7. Fiddy, S. G.; Bogdanchikova, N. E.; Petranovskii, V. P.; Ogden, J. S.; Avalos-Borja, M., EXAFS and optical spectroscopy characterisation of silver within zeolite matrices. In *Stud. Surf. Sci. Catal.*, Aiello, R.; Giordano, G.; Testa, F., Eds. Elsevier: 2002; Vol. 142, pp 1939-1946.
8. Karge, H. G.; Geidel, E., Vibrational Spectroscopy. In *Characterization I: -/-*, Karge, H. G.; Weitkamp, J., Eds. Springer Berlin Heidelberg: Berlin, Heidelberg, 2004; pp 1-200.
9. Sayah, E.; Brouri, D.; Massiani, P., A comparative in situ TEM and UV–visible spectroscopic study of the thermal evolution of Ag species dispersed on Al2O3 and NaX zeolite supports. *Catal. Today* **2013,** *218-219*, 10-17.
10. Bordiga, S.; Regli, L.; Cocina, D.; Lamberti, C.; Bjørgen, M.; Lillerud, K. P., Assessing the Acidity of High Silica Chabazite H−SSZ-13 by FTIR Using CO as Molecular Probe: Comparison with H−SAPO-34. *J. Phys. Chem. B* **2005,** *109* (7), 2779-2784.
11. Bordiga, S.; Regli, L.; Lamberti, C.; Zecchina, A.; Bjørgen, M.; Lillerud, K. P., FTIR Adsorption Studies of H2O and CH3OH in the Isostructural H-SSZ-13 and H-SAPO-34: Formation of H-Bonded Adducts and Protonated Clusters. *J. Phys. Chem. B* **2005,** *109* (16), 7724-7732.
12. Sadlo, J.; Danilczuk, M.; Michalik, J., Interaction of tetrameric silver with ammonia in AgCs-rho zeolite. *Phys. Chem. Chem. Phys.* **2001,** *3* (9), 1717-1720.
13. Jentys, A.; Warecka, G.; Lercher, J. A., Surface chemistry of H-ZSM5 studied by time-resolved IR spectroscopy. *J. Mol. Catal.* **1989,** *51* (3), 309-327.
14. Alonso-Escobar, C. Estudio de materiales zeolíticos como estructuras anfitrionas de nanopartículas: aplicaciones catalíticas y medioambientales. Universitat Politècnica de València, 2017.